

Operation of slope-assisted Brillouin optical correlation-domain reflectometry: comparison of system output with actual frequency shift distribution

HEEYOUNG LEE,^{1,*} NEISEI HAYASHI,² YOSUKE MIZUNO,¹ AND KENTARO NAKAMURA¹

¹*Institute of Innovative Research, Tokyo Institute of Technology, 4259, Nagatsuta-cho, Midori-ku, Yokohama 226-8503, Japan*

²*Research Center for Advanced Science and Technology, The University of Tokyo, 4-6-1, Komaba, Meguro-ku, Tokyo 153-8904, Japan*

*hylee@sonic.pi.titech.ac.jp

Abstract: Although the proof of concept for slope-assisted (SA-) Brillouin optical correlation-domain reflectometry (BOCDR) has been demonstrated, no reports on its detailed operation have been provided to date. We theoretically and experimentally investigate the relationship between the system output (power-change distribution) of SA-BOCDR and the actual Brillouin frequency shift (BFS) distribution along the sensing fiber and show that these two are not identical. When the strained fiber section is much longer than the nominal spatial resolution, the actual distribution of the BFS (i.e., strain) is well reproduced by the power-change distribution. However, when the length of the strained section is equal to or only a few times the nominal resolution, the correct BFS distribution cannot be directly obtained. Even when the strained section is shorter than the nominal resolution, a shift in the power change can still be observed, which is not the case for standard BOCDR systems. This unique “beyond-nominal-resolution” effect will be of great use in practical applications.

© 2016 Optical Society of America

OCIS codes: (060.2370) Fiber optics sensors; (120.0280) Remote sensing and sensors; (280.4788) Optical sensing and sensors.

References and links

1. X. Bao and L. Chen, “Recent progress in distributed fiber optic sensors,” *Sensors (Basel)* **12**(7), 8601–8639 (2012).
2. R. K. Yamashita, Z. He, and K. Hotate, “Spatial resolution improvement in correlation domain distributed measurement of Brillouin grating,” *IEEE Photonics Technol. Lett.* **26**(5), 473–476 (2014).
3. H. J. Park and M. H. Song, “Linear FBG temperature sensor interrogation with Fabry-Perot ITU multi-wavelength reference,” *Sensors (Basel)* **8**(10), 6769–6776 (2008).
4. G. P. Agrawal, *Nonlinear Fiber Optics* (Academic Press, California, 1995).
5. T. Horiguchi and M. Tateda, “BOTDA–nondestructive measurement of single-mode optical fiber attenuation characteristics using Brillouin interaction: theory,” *J. Lightwave Technol.* **7**(8), 1170–1176 (1989).
6. W. Li, X. Bao, Y. Li, and L. Chen, “Differential pulse-width pair BOTDA for high spatial resolution sensing,” *Opt. Express* **16**(26), 21616–21625 (2008).
7. A. Minardo, R. Bernini, and L. Zeni, “Numerical analysis of single pulse and differential pulse-width pair BOTDA systems in the high spatial resolution regime,” *Opt. Express* **19**(20), 19233–19244 (2011).
8. Y. Dong, L. Chen, and X. Bao, “Time-division multiplexing-based BOTDA over 100 km sensing length,” *Opt. Lett.* **36**(2), 277–279 (2011).
9. Y. Peled, A. Motil, I. Kressel, and M. Tur, “Monitoring the propagation of mechanical waves using an optical fiber distributed and dynamic strain sensor based on BOTDA,” *Opt. Express* **21**(9), 10697–10705 (2013).
10. D. Garus, T. Gogolla, K. Krebber, and F. Schliep, “Distributed sensing technique based on Brillouin optical-fiber frequency-domain analysis,” *Opt. Lett.* **21**(17), 1402–1404 (1996).
11. R. Bernini, A. Minardo, and L. Zeni, “Distributed sensing at centimeter-scale spatial resolution by BOFDA: Measurements and signal processing,” *IEEE Photonics J.* **4**(1), 48–56 (2012).
12. A. Minardo, R. Bernini, and L. Zeni, “A simple technique for reducing pump depletion in long-range distributed Brillouin fiber sensors,” *IEEE Sens. J.* **9**(6), 633–634 (2009).
13. K. Hotate and T. Hasegawa, “Measurement of Brillouin gain spectrum distribution along an optical fiber using a

- correlation-based technique—Proposal, experiment and simulation—,” IEICE Trans. Electron. **E83-C**(3), 405–412 (2000).
14. W. Zou, C. Jin, and J. Chen, “Distributed strain sensing based on combination of Brillouin gain and loss effects in Brillouin optical correlation domain analysis,” *Appl. Phys. Express* **5**(8), 082503 (2012).
 15. C. Zhang, M. Kishi, and K. Hotate, “5,000 points/s high-speed random accessibility for dynamic strain measurement at arbitrary multiple points along a fiber by Brillouin optical correlation domain analysis,” *Appl. Phys. Express* **8**(4), 042501 (2015).
 16. J. H. Jeong, K. H. Chung, S. B. Lee, K. Y. Song, J. M. Jeong, and K. Lee, “Linearly configured BOCDA system using a differential measurement scheme,” *Opt. Express* **22**(2), 1467–1473 (2014).
 17. K. Y. Song, M. Kishi, Z. He, and K. Hotate, “High-repetition-rate distributed Brillouin sensor based on optical correlation-domain analysis with differential frequency modulation,” *Opt. Lett.* **36**(11), 2062–2064 (2011).
 18. T. Kurashima, T. Horiguchi, H. Izumita, S. Furukawa, and Y. Koyamada, “Brillouin optical-fiber time domain reflectometry,” *IEICE Trans. Commun.* **E76-B**(4), 382–390 (1993).
 19. D. Iida and F. Ito, “Detection sensitivity of Brillouin scattering near Fresnel reflection in BOTDR measurement,” *J. Lightwave Technol.* **26**(4), 417–424 (2008).
 20. M. Ohsaki, M. Tateda, T. Omatsu, and H. Ohno, “Spatial resolution enhancement of distributed strain measurement using BOTDR by partially gluing optical fiber,” *IEICE Trans. Commun.* **E85-B**(8), 1636–1639 (2002).
 21. N. Nitta, M. Tateda, and T. Omatsu, “Spatial resolution enhancement in BOTDR by spectrum separation method,” *Opt. Rev.* **9**(2), 49–53 (2002).
 22. Y. Koyamada, Y. Sakairi, N. Takeuchi, and S. Adachi, “Novel technique to improve spatial resolution in Brillouin optical time-domain reflectometry,” *IEEE Photonics Technol. Lett.* **19**(23), 1910–1912 (2007).
 23. Y. Mizuno, W. Zou, Z. He, and K. Hotate, “Proposal of Brillouin optical correlation-domain reflectometry (BOCDR),” *Opt. Express* **16**(16), 12148–12153 (2008).
 24. Y. Mizuno, Z. He, and K. Hotate, “Measurement range enlargement in Brillouin optical correlation-domain reflectometry based on temporal gating scheme,” *Opt. Express* **17**(11), 9040–9046 (2009).
 25. Y. Mizuno, Z. He, and K. Hotate, “Measurement range enlargement in Brillouin optical correlation-domain reflectometry based on double-modulation scheme,” *Opt. Express* **18**(6), 5926–5933 (2010).
 26. Y. Mizuno, Z. He, and K. Hotate, “Distributed strain measurement using a tellurite glass fiber with Brillouin optical correlation-domain reflectometry,” *Opt. Commun.* **283**(11), 2438–2441 (2010).
 27. S. Manotham, M. Kishi, Z. He, and K. Hotate, “1-cm spatial resolution with large dynamic range in strain distributed sensing by Brillouin optical correlation domain reflectometry based on intensity modulation,” *Proc. SPIE* **8351**, 835136 (2012).
 28. Y. Mizuno and K. Nakamura, “Experimental study of Brillouin scattering in perfluorinated polymer optical fiber at telecommunication wavelength,” *Appl. Phys. Lett.* **97**(2), 021103 (2010).
 29. N. Hayashi, Y. Mizuno, and K. Nakamura, “Distributed Brillouin sensing with centimeter-order spatial resolution in polymer optical fibers,” *J. Lightwave Technol.* **32**(21), 3999–4003 (2014).
 30. Y. Mizuno, N. Hayashi, H. Fukuda, K. Y. Song, and K. Nakamura, “Ultrahigh-speed distributed Brillouin reflectometry,” *Light Sci. Appl.* **5**, e16184 (2016).
 31. Y. Peled, A. Motil, L. Yaron, and M. Tur, “Slope-assisted fast distributed sensing in optical fibers with arbitrary Brillouin profile,” *Opt. Express* **19**(21), 19845–19854 (2011).
 32. X. Tu, H. Luo, Q. Sun, X. Hu, and Z. Meng, “Performance analysis of slope-assisted dynamic BOTDA based on Brillouin gain or phase-shift in optical fibers,” *J. Opt.* **17**(10), 105503 (2015).
 33. A. Minardo, A. Coscetta, R. Bernini, and L. Zeni, “Heterodyne slope-assisted Brillouin optical time-domain analysis for dynamic strain measurements,” *J. Opt.* **18**(2), 025606 (2016).
 34. H. Lee, N. Hayashi, Y. Mizuno, and K. Nakamura, “Slope-assisted Brillouin optical correlation-domain reflectometry: proof of concept,” *IEEE Photonics J.* **8**(3), 6802807 (2016).
 35. Y. Mizuno, W. Zou, Z. He, and K. Hotate, “Operation of Brillouin optical correlation-domain reflectometry: theoretical analysis and experimental validation,” *J. Lightwave Technol.* **28**(22), 3300–3306 (2010).
 36. K. Y. Song, Z. He, and K. Hotate, “Effects of intensity modulation of light source on Brillouin optical correlation domain analysis,” *J. Lightwave Technol.* **25**(5), 1238–1246 (2007).
 37. S. Takahashi and S. Shibata, “Thermal variation of attenuation for optical fibers,” *J. Non-Cryst. Solids* **30**(3), 359–370 (1979).

1. Introduction

Due to increasing demand for structural health monitoring of civil infrastructure, a variety of fiber-optic sensors have been extensively studied [1–3]. In particular, distributed optical fiber sensors based on Brillouin scattering [4] have been receiving considerable attention due to their measurement capabilities for strain and temperature change. Hence, many types of Brillouin-based measurement schemes have been developed, including Brillouin optical time-, frequency-, and correlation-domain analysis (BOTDA [5–9], BOFDA [10–12], and BOCDA [13–17]), and Brillouin optical time- and correlation-domain reflectometry (BOTDR [18–22] and BOCDR [23–30]). Each scheme is being extensively studied and has its own advantages

and disadvantages; here, we focus on BOCDR, which has a high spatial resolution and operates by single-end light injection.

Since the basic BOCDR system was first proposed in 2008 [23], numerous configurations have been implemented in order to improve its performance [24–34]. For example, the measurement range was elongated using temporal gating [24] and double modulation [25]; millimeter-order spatial resolution was achieved by use of a tellurite glass fiber [26] and by apodization [27]; and the strain dynamic range was extended using polymer optical fibers [28, 29]. In addition, one of the latest breakthroughs is phase-detection-based BOCDR [30], which enables a high sampling rate of >100 kHz per point. We have recently developed another high-speed configuration, motivated by previous implementations in the time domain [31–33], called slope-assisted (SA-) BOCDR [34], in which the spectral power of the Brillouin gain spectrum (BGS) is exploited to deduce the Brillouin frequency shift (BFS). This configuration can potentially allow for higher-speed operation than the phase-detection-based method, and for detection of not only changes in strain and temperature, but also optical losses, if necessary. Although the proof of concept for SA-BOCDR has been demonstrated [34], there is still much room for performance improvement. One fundamental issue that must be solved in order to characterize SA-BOCDR operation is the correspondence between the final system output (i.e., power-change distribution) and the actual BFS distribution. In standard BOCDR systems based on frequency information, these two distributions have been proven to be identical, in principle; however, in an SA-BOCDR system based on power information, no report has been made so far.

In this paper, we theoretically and experimentally show that the final system output of SA-BOCDR is generally different from the actual BFS distribution. When the strained section is sufficiently longer than the nominal spatial resolution, the power-change distribution almost reproduces the actual BFS (or strain) distribution. However, when the strained section is almost equal to or only a few times longer than the nominal resolution, the actual BFS distribution is not directly obtained (further data processing is necessary). We also show that even when the strained section is shorter than the nominal resolution some shift in the power change can be observed. This feature is unique to SA-BOCDR and potentially useful for practical applications.

2. Principle

In general, fiber-optic distributed Brillouin sensors operate based on the dependence of the BFS on strain and temperature [4]. As mentioned above, BOCDR is the only technique with intrinsic single-end accessibility and a relatively high spatial resolution. It resolves the sensing locations using a so-called correlation peak [23], which can be generated in the fiber under test (FUT) via sinusoidal frequency modulation of the laser output. The location of the correlation peak can be scanned for along the FUT by sweeping the modulation frequency f_m ; thus, distributed BFS measurement becomes feasible. Sinusoidal frequency modulation results in the periodic generation of multiple correlation peaks along the FUT, and their frequency determines the measurement range d_m by [35]

$$d_m = \frac{c}{2n f_m}, \quad (1)$$

where c is the velocity of light in vacuum and n is the core refractive index. When f_m is lower than the Brillouin bandwidth $\Delta\nu_B$, the spatial resolution Δz is given by [35]

$$\Delta z = \frac{c \Delta\nu_B}{2\pi n f_m \Delta f}, \quad (2)$$

where Δf is the modulation amplitude of the optical frequency.

In conventional BOCDR, the BFS at one sensing position is determined from a peak frequency after the acquisition of the whole BGS [23, 35], while in SA-BOCDR, it is obtained using the spectral power change at a fixed frequency, by exploiting its one-to-one correspondence with the BFS [34]. Consequently, the BFS distribution along the FUT is obtained as a power-change distribution in SA-BOCDR. The measurement range and the spatial resolution are given by the same equations as are used for standard BOCDR (Eqs. (1) and (2)). Note that with this scheme, loss points can also be detected in a distributed manner and the sampling rate can potentially be drastically enhanced (refer to Ref. 18 for the detailed operating principle of SA-BOCDR).

3. Simulation

We simulated the system output of SA-BOCDR. We assumed that one section of the FUT was uniformly strained. The magnitude of the strain was assumed to constantly lie below the upper limit of the linear region ($\sim 2000 \mu\epsilon$) [34]. The length of the strained section was set to $0.25R$, $0.5R$, $0.75R$, R , $2R$, $5R$, and $10R$, where R indicates the nominal spatial resolution calculated using Eq. (2). First, the simulation results for the strain distributions acquired using standard BOCDR (deduced from the BFS distributions using the linear BFS-to-strain relationship) are shown in Fig. 1(a), which completely reproduce the actual BFS distributions. Next, the simulation results for the strain distributions obtained from SA-BOCDR (also deduced from the final power-change distributions simply based on the linear power-to-strain relationship) are shown in Fig. 1(b) (strained: $0.5R$, R , $2R$, $5R$, and $10R$) and Fig. 1(c) (strained: $0.25R$, $0.5R$, $0.75R$, and R). Here, for simplicity, we neglected both the complicated longitudinal shape of the correlation peak and the influence of its sidelobes [36]; that is, the longitudinal shape of the correlation peak was approximated by a rectangular profile with a length of R . At the ends of the strained section (i.e., the boundaries between the strained and non-strained sections), the power change varied linearly with the length of R ; consequently, each whole power-change distribution showed a trapezoidal shape (including triangular). Thus, we see that when the strained section is sufficiently longer than R , the power-change distribution almost reproduces the actual BFS distribution. In contrast, when the length of the strained section is approximately R or only a few times longer than R , the correct BFS distribution cannot be directly obtained (under the assumption that the strain is uniformly applied; however, the correct information can be easily derived). What is notable here is that even when the strained section is shorter than R , we can observe a trapezoidal-shaped shift in the power change and thereby obtain the information that some irregularity has occurred at that point. For instance, when the length of the strained section is $0.5R$, a trapezoidal shape with a maximal power-change shift corresponding to half the amount seen with a strained section longer than R is observed. This “beyond-nominal-resolution” information, which neither standard BOCDR systems nor SA-BOTDR/BOTDA systems can provide (note that standard BOCDR systems determine the BFS as the frequency at which the highest spectral peak is observed; even when the local Brillouin spectrum includes a low spectral peak corresponding to strain, as long as this peak is lower than the initial spectral peak corresponding to the non-strained sections, it does not contribute to the derived BFS), will be of great use in practical applications. One important benefit is that using this effect, we can effectively elongate the measurement range of BOCDR, which generally suffers from the trade-off relation between the spatial resolution and the measurement range.

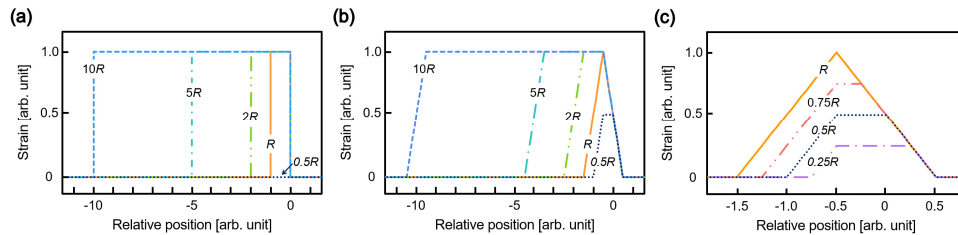


Fig. 1. Deduced strain distributions directly obtained from the final power outputs of (a) standard BOCDR and (b, c) SA-BOCDR. Note that the traces in (a) give the correct strain distributions.

4. Experimental setup

The experimental setup for SA-BOCDR used to evaluate the aforementioned simulation results is shown schematically in Fig. 2(a), following the same basic setup as previously reported [34]. The light output from a $1.55\ \mu\text{m}$ laser was divided into pump and reference beams. The pump beam was guided through a polarization scrambler (PSCR) to suppress the polarization-dependent signal fluctuations, then amplified to $\sim 27\ \text{dBm}$ using an erbium-doped fiber amplifier (EDFA) and injected into the FUT. The backscattered Stokes light was amplified to $\sim 2\ \text{dBm}$ using another EDFA. The reference beam was guided through a $\sim 1\text{-km}$ -long delay line and amplified to $\sim 1\ \text{dBm}$. The Stokes and the reference beams were then mixed (heterodyned), converted into an electrical signal using a photo diode (PD), and guided to an electrical spectrum analyzer (ESA). Using the narrow band-pass filtering function of the ESA (with the video bandwidth and resolution bandwidth set to $10\ \text{kHz}$ and $10\ \text{MHz}$, respectively), the change in the spectral power at $10.81\ \text{GHz}$ was sequentially output to an oscilloscope (OSC). An electrical amplifier was not used in this measurement.

The FUT was a 13.0-m -long single-mode silica fiber with a BFS of $10.86\ \text{GHz}$ at $1.55\ \mu\text{m}$ at room temperature. Measurements were performed using two configurations: one for a relatively high spatial resolution and the other for a relatively low resolution (required to investigate the beyond-nominal-resolution effect). In the first, high-resolution configuration, strains of $750\ \mu\epsilon$ and $1500\ \mu\epsilon$ were applied to 5-cm -, 10-cm -, 20-cm -, 50-cm -, and 100-cm -long sections of the FUT, as depicted in Fig. 2(b). The modulation frequency f_m and amplitude Δf were set to $7.11\text{--}7.31\ \text{MHz}$ and $1.3\ \text{GHz}$, respectively, corresponding to the measurement range of $14.5\ \text{m}$ and the theoretical spatial resolution of $9.5\ \text{cm}$ according to Eqs. (1) and (2). In the second, low-resolution configuration, a strain of $1500\ \mu\epsilon$ was applied to 5-cm -, 10-cm -, 15-cm -, and 20-cm -long sections of the FUT (see Fig. 2(c)). The modulation frequency f_m was swept in the same range ($7.11\text{--}7.31\ \text{MHz}$), thus giving the same measurement range ($14.5\ \text{m}$). The modulation amplitude Δf was reduced to $0.7\ \text{GHz}$, corresponding to a theoretical spatial resolution of $19.6\ \text{cm}$. In both configurations, the repetition rate was set to $100\ \text{Hz}$, and 64 times averaging was performed on the OSC to improve the signal-to-noise ratio (SNR). The room temperature was $25\ ^\circ\text{C}$.

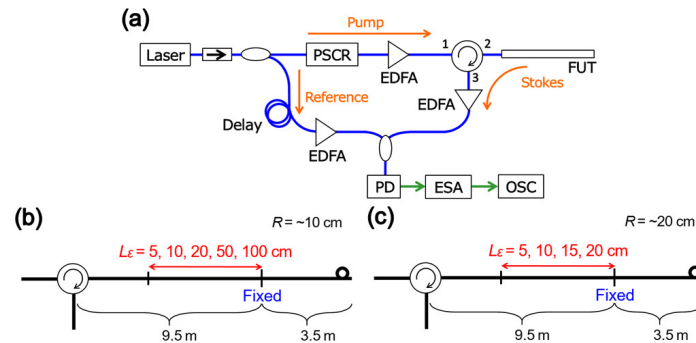


Fig. 2. (a) Experimental setup for SA-BOCDR, which is basically the same as Fig. 3 of Ref. 34. EDFA: erbium-doped fiber amplifier, ESA: electrical spectrum analyzer, FUT: fiber under test, OSC: oscilloscope, PD: photo diode, PSCR: polarization scrambler. The blue curves indicate silica fibers, and the green lines indicate electrical cables. (b) Structure of an FUT with a relatively high spatial resolution (9.5 cm). (c) Structure of an FUT with a relatively low spatial resolution (19.6 cm).

5. Experimental results

First, we present the experimental results with relatively high spatial resolution (9.5 cm). An example of the measured power change distribution (converted into strain) along the whole length of the FUT (with a $1500 \mu\epsilon$ strain applied to a 20-cm-long section) is shown in Fig. 3(a). At this scale, it appears that the correct amount of strain was detected at the correct location. The strain distributions measured when strains of $750 \mu\epsilon$ and $1500 \mu\epsilon$ were applied (magnified views around the strained sections), simply deduced from the power-change distributions based on the linear power-to-strain relationship, are shown in Fig. 3(b) and 3(c), respectively. Each distribution is shifted by $3000 \mu\epsilon$, and the simulated data is indicated by dotted lines. The trends in the measured distributions agree well with the simulation results, including the case where the strained section is half the nominal spatial resolution. This indicates that our relatively rough simulation is almost sufficient to predict the experimental results, which is beneficial from the viewpoint of simulation cost. The discrepancy from the simulation results probably originates from signal fluctuations due to an insufficient SNR and the fact that the influence of the correlation peak sidelobes was not considered in the simulation process.

Subsequently, we performed similar experiments with a relatively low spatial resolution (19.6 cm) to evaluate the beyond-nominal-resolution effect. The magnified views of the strain distributions (simply deduced from the power-change distributions), measured when a strain of $1500 \mu\epsilon$ was applied, are shown in Fig. 4. As the strained section becomes shorter, the maximal power-change shift becomes smaller. The trend in the measured distributions is basically in good agreement with the simulation results. As the strained section is shortened further, the signal is buried by the noise. The standard deviation of the noise floor (power fluctuations corresponding to the strain of the non-strained sections) was calculated to be approximately $130 \mu\epsilon$ in this measurement. This amount is theoretically obtained as the maximal strain when the strained section is 1.7 cm, which could be regarded as the shortest detectable length. Note that this value is influenced by various experimental parameters such as the amount of the actual strain, the number of averaging, the incident power, etc.

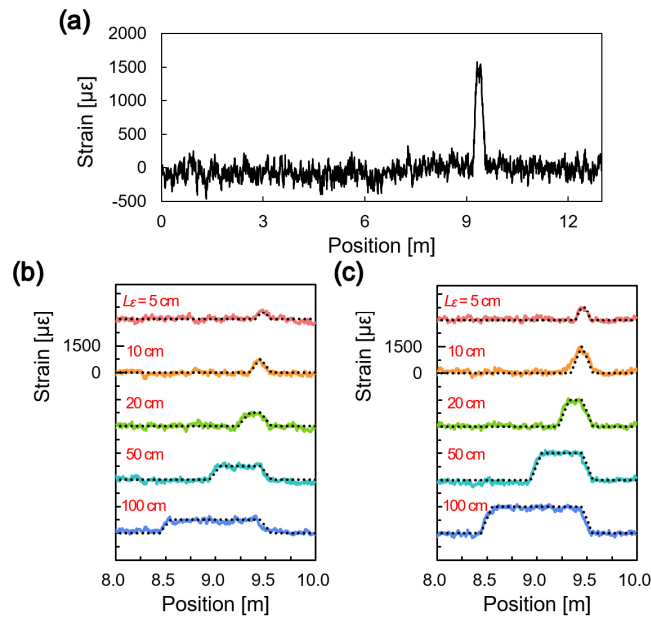


Fig. 3. Deduced strain distributions with a spatial resolution of 9.5 cm: (a) example measurement along the whole length of the FUT when a 1500 $\mu\epsilon$ strain was applied to a 20-cm-long section, and magnified views when strains of (b) 750 $\mu\epsilon$ and (c) 1500 $\mu\epsilon$ were applied to 5-cm- to 100-cm-long sections. In (b) and (c), each distribution was shifted by 3000 $\mu\epsilon$, and the dotted lines indicate the simulated data.

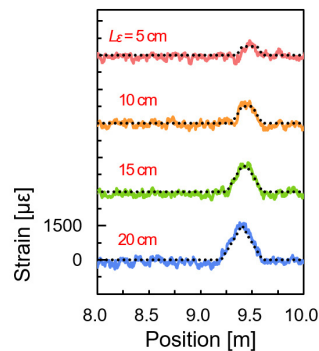


Fig. 4. Magnified views of the deduced strain distributions with a spatial resolution of 19.6 cm; a 1500 $\mu\epsilon$ strain was applied to 5-cm- to 20-cm-long sections. Each distribution was shifted by 3000 $\mu\epsilon$, and the dotted lines indicate the simulated data.

6. Conclusions

The final system output (i.e., the power-change distribution) of the SA-BOCDR system has been shown, both theoretically and experimentally, not to reproduce the actual BFS (or strain) distribution. When the strained section was sufficiently longer than the nominal spatial resolution, the system output almost corresponded to the actual BFS distribution. In contrast, when the length of the strained section was equal to or only a few times the nominal resolution, the BFS distribution was not reproduced correctly. These findings will be of great importance in improving the performance of SA-BOCDR systems in the future. In addition, we have also demonstrated that a strained section that is even shorter than the nominal resolution can still be detected as a shift in the power change. Beyond-nominal-resolution sensing of temperature change will be also feasible in the same way (cf. the influence of

thermal expansion [37] is smaller than the noise floor fluctuations in this measurement). As for loss sensing, as it is point detection, the same effect cannot be observed (not available); in theory, the measured power gradually changes along the length equal to the nominal resolution. We anticipate that this feature, unique to SA-BOCDR, will be an attractive advantage in every application where even slight strain or heat cannot be permitted (regarded as irregular) because of the required high-level constancy, such as nuclear plant monitoring.

Funding

JSPS KAKENHI (25709032, 26630180, 25007652); Iwatani Naoji Foundation; SCAT Foundation; Konica Minolta Science and Technology Foundation.